J Opt (June 2017) 46(2):149–157
DOI 10.1007/s12596-016-0351-4

RESEARCH ARTICLE

Synthesis, growth, structural, thermal, dielectric, linear and nonlinear optical studies of 2-amino 6-methylpyridinium salicylate single crystal

S. Venda[1] · G. Peramaiyan[2] · M. NizamMohideen[3] · G. Vinitha[4] · S. Srinivasan[1]

Received: 28 October 2015 / Accepted: 9 June 2016 / Published online: 22 June 2016

Abstract Single crystal of 2-amino 6-methylpyridinium salicylate (2A6MPS) was grown for the first time by the slow evaporation method. Single crystal X-ray diffraction analysis was employed to estimate the cell parameters of the grown crystal. The third order nonlinear optical properties of 2A6MPS was studied by the *Z*-scan technique using 532 nm diode pumped CW Nd:YAG laser. Nonlinear refractive index, nonlinear absorption coefficient and nonlinear susceptibility of the grown crystal were found to be 10^{-8} cm^2/W, 10^{-4} cm/W and 10^{-6} esu, respectively. Thermal stability of 2A6MPS was studied by thermogravimetry (TG) and differential thermal analyses (DTA). The optical transmittance window and the lower cut-off wavelength of 2A6MPS were identified by UV–Vis–NIR studies. From the dielectric measurements, the relative dielectric permittivities ε_{11} and ε_{33} values were determined.

Keywords Crystal structure · Crystal morphology · Growth from solutions · Single crystal growth · Organic compounds · Nonlinear optical materials

✉ S. Srinivasan
dr_s_srinivasan@yahoo.com

[1] Department of Physics, Presidency College, Chennai 600005, India

[2] Department of Physics, Vel Tech University, Chennai 600062, India

[3] Department of Physics, The New College (Autonomous), Chennai 600014, India

[4] Department of Physics, VIT University, Chennai 600127, India

Introduction

In recent years, nonlinear optical (NLO) crystals have been a great deal of interest due to their potential applications in the domain of optoelectronics and photonic technologies. Pyridine derivatives with large π-electron delocalization have received much attention from materials scientists due to its large second and third order nonlinearities. Crystal engineering provides clear information about the molecular design and intermolecular interactions of constituent molecules in the crystal packing. It paves the way to utilize such perception in the design of novel materials with desired properties [1–3]. Acentric and centric organic crystals with large π-electron delocalization are preferred for second and third order nonlinear optical applications. Because, optical nonlinearity depends on the crystal symmetry. As the control of molecular orientation in supramolecular structure is tedious and identified as a major obstacle in materials design, many attempts have been made to control the structure of solids through charge transfer, hydrogen bond and π–π interactions [4]. Generally, organic materials possess both donor and acceptor groups with a suitable conjugation path which leads to large third order nonlinearities. The need for efficient third order NLO materials still exist even the importance of second order NLO materials are well understood [5]. Pyridine derivatives are present in many large molecules having photo-chemical, electro-chemical and catalytic applications. Due to the strong base character of 2-amino-6-methylpyridine, the nitrogen atom of it accepts proton from other carboxylic acids forming a 2-amino-6-methylpyridinium cation. Recently, many aminopyridinium complexes with excellent nonlinear optical properties have been reported [6]. In the present work, a novel organic 2-amino 6-methylpyridinium salicylate compound

was synthesized by a slow evaporation solution growth technique for the first time. The solubility, crystal morphology, structural as well as thermal, dielectric, optical and third-order nonlinear optical properties of 2A6MPS were reported for the first time.

Experimental

Synthesis, solubility and crystal growth

Commercially available 2-amino-6-methylpyridine and salicylic acid were taken in an equimolar ratio and dissolved in methanol at room temperature. The prepared solution was allowed for stirring about 3 h using a temperature controlled magnetic stirrer.

The synthesized salt was purified by successive recrystallization process using methanol as a solvent. During the reaction, a proton is transferred from the electron donor group of salicylic acid to the electron acceptor group of 2-amino 6-methylpyridine resulting 2-amino-6-methylpyridinium salicylate compound. The title salt was synthesized according to the following reaction scheme as shown in Fig. 1.

Solvent selection is playing a crucial role for the growth of optically good quality crystals. The solubility of 2-amino-6-methylpyridinium salicylate was assessed in methanol and water + methanol solvents at different temperatures ranging from 35 to 50 °C. 2A6MPS salt was prepared in methanol and water + methanol solvents at 60 °C for the solubility study.

The saturated solution was prepared at different temperatures and the solubility of 2A6MPS was estimated gravimetrically. The obtained solubility curves of 2A6MPS in the two solvents are shown in Fig. 2. From the solubility studies, it is found that the title compound exhibits positive solubility gradient in both solvents. The recrystallized salt of 2A6MPS was used for the preparation of saturated solution at 35 °C using methanol solvent. Then, the prepared solution was filtered and covered with a perforated sheet to restrict the fast evaporation of the solvent.

The prepared growth solution was kept in a constant temperature bath with an accuracy of ±0.01 °C. After a span of 35 days, crystals with well defined facets have been harvested but the crystals are opaque in nature (Fig. 3a). So, the harvested crystals from the methanolic solution were dissolved using a mixture of methanol (50 %) and water (50 %) solvents and then the growth solution was kept in a constant temperature water bath at the temperature of 35 °C. After a period of 18 days, optically transparent crystals were harvested as shown in Fig. 3b.

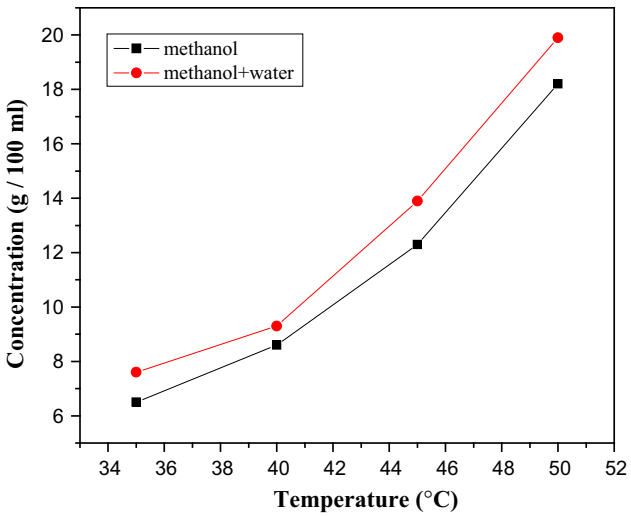

Fig. 2 Solubility curves of 2A6MPS in methanol and methanol + water solvents

Results and discussion

Single crystal X-ray diffraction and morphological studies

The crystal structure details of 2-amino-6-methylpyridinium salicylate were determined by single crystal X-ray diffraction method. The intensity data were collected using a Bruker kappa APEXII single crystal X-ray diffractometer with a graphite monochromated MoK_{α} radiation ($\lambda = 0.71073$ Å) at 293 K [7]. The structure was solved by the direct method and refined by the full matrix least-squares technique on F^2 employing the SHELXL 97 program package [8]. The crystallographic data of 2A6MPS

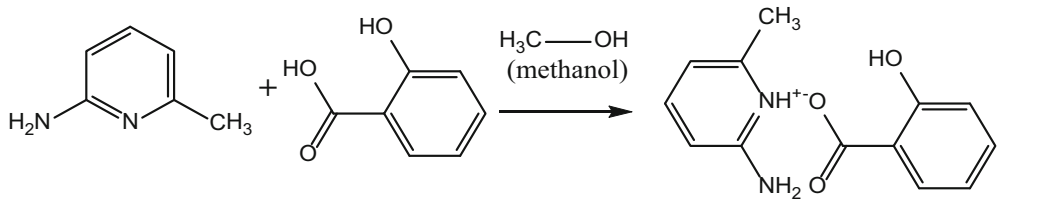

2-amino-6-methylpyridine salicylic acid 2-amino6methylpyridinium salicylate

Fig. 1 Reaction scheme of 2A6MPS

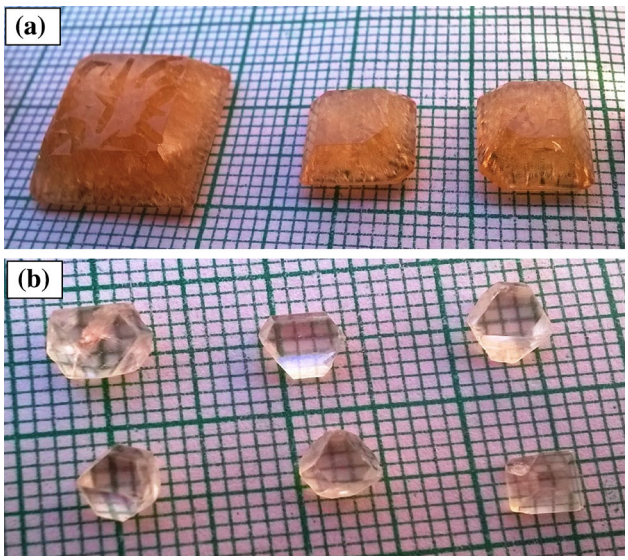

Fig. 3 As-grown crystal of 2A6MPS using **a** methanol solvent. **b** methanol + water solvent

crystal are listed in Table 1. The asymmetric unit of the title compound comprises of a 2-amino 6-methylpyridinium cation and salicylate anion as shown in the ORTEP diagram (Fig. 4). The packing diagram of 2-amino-6-methylpyridinium salicylate is show in Fig. 5. The molecular formula of the crystal is $C_{13}H_{14}N_2O_3$. 2A6MPS crystallizes in a tetragonal crystal system with space group I41/a. The cell parameters are a = 14.086(5) Å, b = 14.086(5) Å, c = 24.621(5) Å, α, β and γ = 90.000(5)° and volume V = 4885(3) Å^3. Protonation at N position have taken place from the hydrogen atom of the carboxyl group of the salicylic acid. The protonation at N1 of 2-amino 6-methylpyridinium resulted in the widening of C9–N1–C13 angle of the pyridinium ring to 123.1(2)°, compared to 115.25(13)° in unprotonated aminopyridine [9]. This type of protonation is observed in various aminopyridine acid complexes [10–12]. The 2-amino-6-methylpyridinium cation and salicylate anion are having a maximum deviation of 0.001(2) Å for atom C11 and 0.002(3) Å for atom C2, respectively. The dihedral angle between these two planes is about 14.72(8)°. The bond lengths and angles are within the expected range [13]. In the cation, the N2–C9 [1.318(3) Å] bond is shorter than the N1–C9 [1.347(3) Å] and N1–C13 [1.363(3) Å] bonds, and the C9–C10 [1.401(4) Å] and C11–C12 [1.392(4) Å] bonds lengths are significantly longer than bonds C10–C11 [1.337(4) Å] and C12–C13 [1.354(4) Å], similar to those observed previously for the aminopyridinium cation. In contrast, in the solid state structure of aminopyridinium, the C–N(H_2) bond is clearly longer than that in the ring [14]. The geometrical features of the amino-pyridinium cation (N1/N2/C9–C13) resemble those observed in other 2-aminopyridinium structures that are believed to be involved in amine-imine tautomerism [15]. However, previous studies show that a pyridinium cation always possesses an expanded C–N–C angle in comparison with pyridine itself [16]. In the crystal structure, intra as well as intermolecular hydrogen bonds could be observed. The intra-molecular hydrogen bonds are formed by the H atom of the alcoholic hydroxyl group as the donor and the carboxylic O atom of the carboxylic acid group as the acceptor in the salicylate anion (O1–H1···O2), which generates an *S*(6) ring motif. This motif is also observed in the crystal structure of 2-aminopyridinium salicylate [17]. In the crystal packing (Fig. 5), the protonated N1 atom and the 2-amino group (N2) are hydrogen-bonded to the carboxylate oxygen atoms (O2 and O3) via a pair of intermolecular N1–H1A···O2 and N2–H2A···O3 hydrogen bonds forming an $R_2^2(8)$ ring motif. The cation–anion pairs are linked by N2–H2B···O3 hydrogen bonds into chains propagating along [010]. The corresponding data for the hydrogen bonds are listed in Table 2. The morphology of 2A6MPS crystal is shown in Fig. 6.

Thermal studies

The thermal behaviour of 2A6MPS was studied by differential thermal analysis (DTA) and thermogravimetric analysis (TGA) using a NETZSCH STA 409 instrument with a heating rate of 10 °C/min starting from 30 to 600 °C. The TGA trace of 2A6MPS is illustrated in Fig. 7.

A weight loss pattern between 189 and 242 °C is due to the degradation of 2A6MPS compound into gaseous products. Since there is no weight loss up to 188 °C, the crystal is free from solvent molecules in it. In a DT curve, a sharp endotherm at peak 162 °C is assigned to the melting point of 2A6MPS. An endotherm appearing at 242 °C is matched with degradation result of TGA. From the above TG-DT analyses, it is confirmed that the decomposition of 2A6MPS material is just above 188 °C. It is also confirmed that the applicability of this material for any optical device process below 162 °C.

Dielectric studies

The relative dielectric permittivity (ε_r) of 2A6MPSCA crystal was determined using the HIOKI 3532–50 LCR HITESTER instrument. The dielectric permittivity (ε_r) of crystal is a second rank tensor. For tetragonal crystal system, there are two independent tensor components ε_{11} (or) ε_{22} and ε_{33} corresponding to the crystallographic axes 'a' and 'c' respectively. For a tetragonal crystal system ($\alpha = \beta = \gamma = 90°$, $a = b = \varepsilon_{xx} \neq c = \varepsilon_{zz}$) the dielectric permittivity tensor with respect to the crystallographic axes in the conventional orientation is:

Table 1 Crystal data and structure refinement for 2A6MPS

Identification code	2A6MPS
Empirical formula	C_{13} H_{14} N_2 O_3
Formulas weight	246.26
Temperature	293(2) K
Wavelength	0.71073 Å
Crystal system, space group	Tetragonal, I41/a
Unit cell dimensions	a = 14.086(5) Å alpha = 90.000(5)°
	b = 14.086(5) Å beta = 90.000(5)°
	c = 24.621(5) Å gamma = 90.000(5)°
Volume	4885(3) A^3
Z, Calculated density	16, 1.339 Mg/m^3
Absorption coefficient	0.097 mm^{-1}
F(000)	2080
Crystal size	0.30 × 0.20 × 0.20 mm
Theta range for data collection	2.63°–25.00°
Limiting indices	$-16 \leq h \leq 16$, $-16 \leq k \leq 16$, $-29 \leq l \leq 29$
Reflections collected/unique	44214/2158 [R_{int} = 0.0330]
Completeness to theta	25.00 %
Absorption correction	Semi-empirical from equivalents
Max. and min. transmission	0.991 and 0.952
Refinement method	Full-matrix least-squares on F^2
Data/restraints/parameters	2158/0/178
Goodness-of-fit on F^2	1.130
Final R indices [$I > 2\sigma(I)$]	R1 = 0.0457, wR2 = 0.1277
R indices (all data)	R1 = 0.0712, wR2 = 0.1743
Extinction coefficient	0.0010(3)
Largest diff. peak and hole	0.129 and −0.148 e A^{-3}

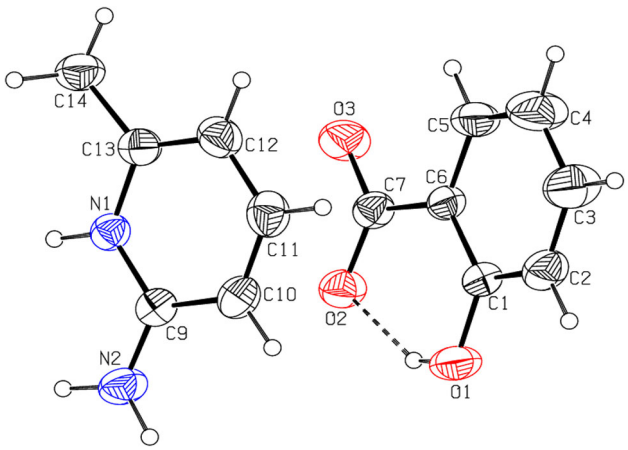

Fig. 4 ORTEP diagram of 2A6MPS crystal

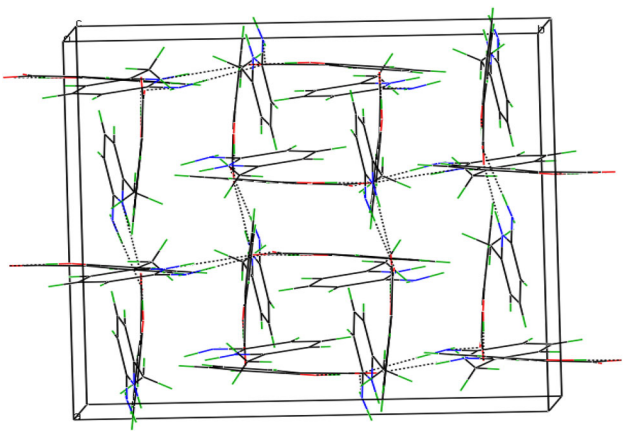

Fig. 5 Packing diagram of 2A6MPS crystal

$$\begin{vmatrix} \varepsilon_{xx} & 0 & 0 \\ 0 & \varepsilon_{xx} & 0 \\ 0 & 0 & \varepsilon_{zz} \end{vmatrix}$$

As-grown crystal of 2A6MPS was cut along (100) and (001) planes with 2 mm thickness of the crystals used. In order to make a parallel plate capacitor, a silver paste was coated on the either side of crystal sample. A relative dielectric permittivity was determined as a function of temperature in the range from 40 to 100 °C at various frequency range (1000 Hz 10 MHz) frequency. The variation of dielectric tensor as a function of temperature is shown in Fig. 8. The determined values of ε_{11}, ε_{33} values

Table 2 Hydrogen bonds of 2A6MPS [Å and °]

D–H···A	d(D–H)	d(H···A)	d(D···A) (DHA)
O(1)–H(1)···O(2)	0.82	1.81	2.541(3) 147.1
N(1)–H(1A)···O(2)	0.93(3)	1.82(3)	2.741(3) 175(2)
N(2)–H(2A)···O(3)	0.92(3)	1.93(3)	2.838(3) 173(2)
N(2)–H(2B)···O(3)	0.93(3)	1.84(3)	2.776(3) 180(3)

Symmetry transformations used to generate equivalent atoms: −x + 2, −y + 1, −z + 1, −y + 5/4, x−1/4, z−1/4

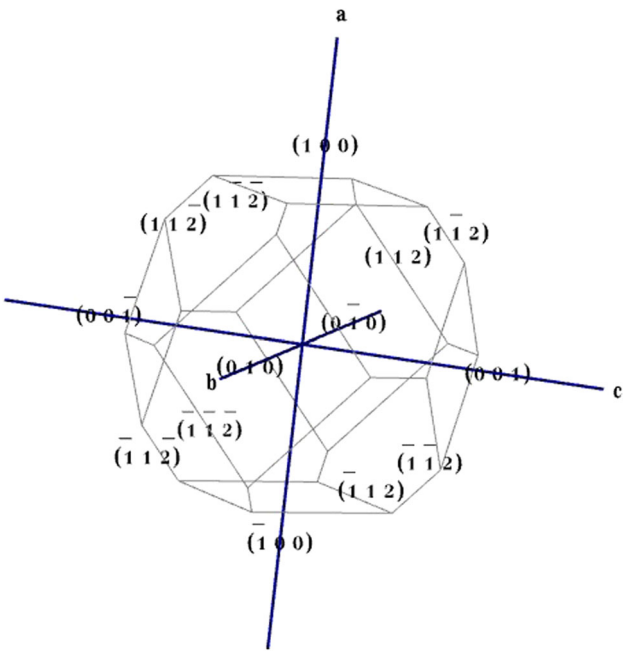

Fig. 6 Morphology of 2A6MPS crystal

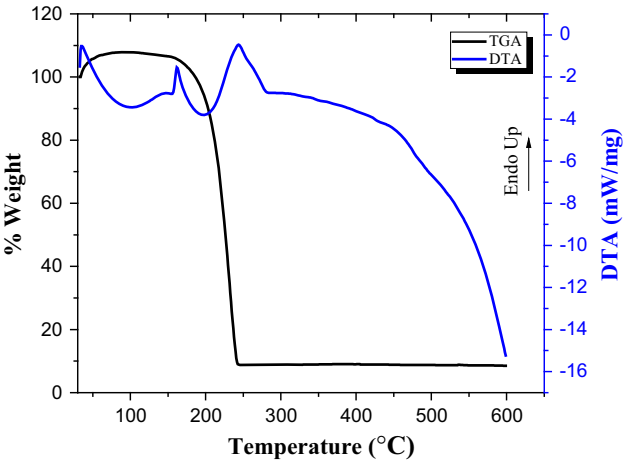

Fig. 7 TG/DTA curves of 2A6MPS

are in the ranges 78.51–77.45 and 80.8–78.65 respectively for the planes (100) and (001). The main panel of Fig. 8 shows the small variation of dielectric permittivity at low temperature and almost constant at higher temperatures without any apparent phase transition, since the 2A6MPS crystal has an inversion centre. The relative dielectric permittivity decreases as the frequency increases and attain constant at higher frequencies [Fig. 8 upper inset (001) plane and lower inset (100) plane], indicating the normal dielectric behavior of 2A6MPS crystal. The low value of dielectric permittivity at higher frequencies shows the presence of four type of polarizations such as electronic, ionic, dipolar and space charge polarizations. The characteristic low values of dielectric loss at high frequencies for the 2A6MPS crystal suggests that the crystal possesses enhanced optical quality with lesser defects and this parameter plays an important role for the fabrication of nonlinear optical devices (Fig. 9) [18]. Hence, it is concluded that 2A6MPS crystal exhibits normal dielectric behavior [19, 20].

UV–Vis–NIR spectral studies

UV–Vis–NIR spectrum provides extensive information about the electronic transition of the π-conjugated molecular systems as the absorption of ultra-violet and visible light involves the promotion of electrons in σ and π-orbitals from the ground state to higher energy states. Figure 10 shows the transmission spectrum of 2A6MPS crystal was recorded in the wavelength range from 190 to 900 nm using a T-90 + LabIndia UV–Vis spectrophotometer. 1 mm thickness of the crystal 2A6MPS was used for this study. The 2A6MPS crystal has sufficient transmittance in the visible region. The optical absorption at 356 nm is due to the promotion of electron from

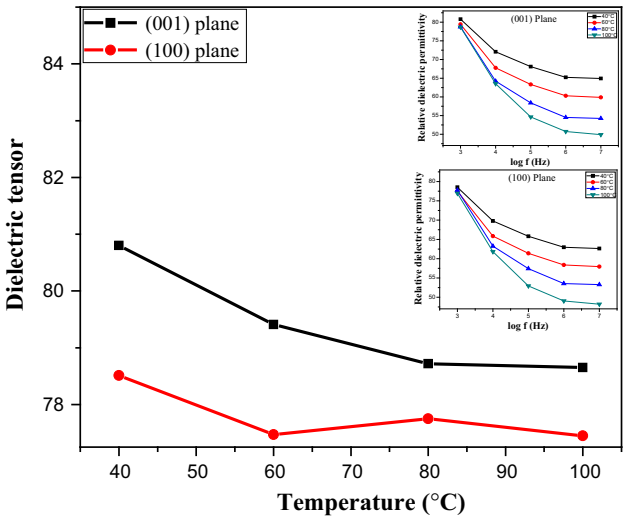

Fig. 8 Plot dielectric tensor versus temperature of 2A6MPS crystal. Relative dielectric permittivity versus log f for (001) plane (*upper inset*). Relative dielectric permittivity versus log f for (100) plane (*lower inset*)

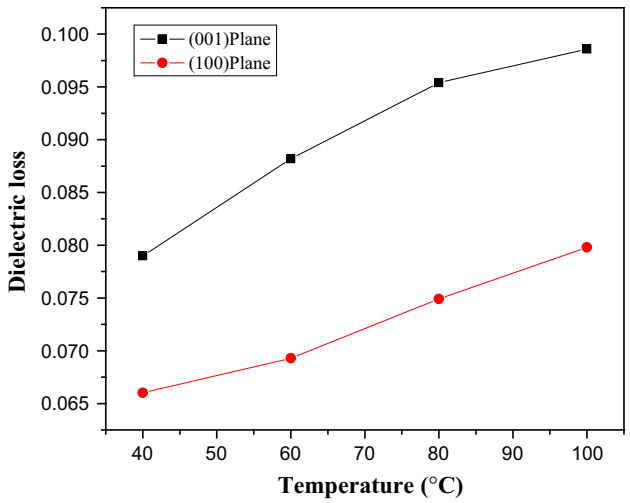

Fig. 9 Plot of dielectric loss versus temperature of 2A6MPS crystal

nonbonding (n) orbital to antibonding orbital (π*). The absorption coefficient (α) can be determined from the transmission (T) spectrum based on the following relations,

$$\alpha = \frac{2.3026}{t}\log(1/T) \quad (1)$$

where T is the transmittance and 't' is the thickness of the crystal.

The reflectance (R) in terms of the absorption coefficient can be derived from the transmission data [21],

$$T = \frac{(1-R)^2 e^{-\alpha t}}{1-R^2 e^{-2\alpha t}} \quad (2)$$

Or,

$$R = \frac{\exp(-\alpha t) \pm \sqrt{\exp(-\alpha t)T - \exp(-3\alpha t)T + \exp(-2\alpha t)T^2}}{\exp(-\alpha t) + \exp(-2\alpha t)T} \quad (3)$$

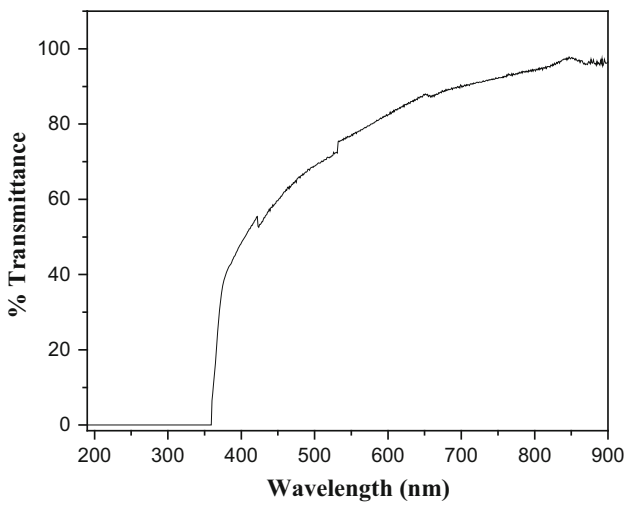

Fig. 10 UV–Vis–NIR transmission spectrum of 2A6MPS crystal

The inset of Fig. 11 shows the reflectance of grown crystal as a fuction of wavelength. It is observed that low transmittance of the crystal is due to high reflectance, showing the good quality of grown crystal.

The optical band gap value was estimated from the transmission spectrum and the optical absorption coefficient (α) near the absorption edge was calculated by the relation,

$$(\alpha h\nu)^2 = A(E_g - h\nu) \quad (4)$$

where E_g is the optical band gap of the crystal and A is a constant. The variation of $(\alpha h\nu)^2$ with hν [22] in the fundamental absorption region was plotted (Fig. 11). The band gap of the crystal estimated by extrapolation of the linear part of the graph was determined to be 3.35 eV.

Nonlinear optical study

The Z-scan technique [23] is a simple but very accurate method to determine both nonlinear index of refraction n_2 and nonlinear absorption coefficient β. Nonlinear index of refraction is proportional to the real part of the third-order susceptibility. [$\mathrm{Re}\chi^{(3)}$] and the nonlinear absorption coefficient is proportional to [$\mathrm{Im}\chi^{(3)}$]. The *Z*-scan experiments were performed using a 532 nm diode pumped CW Nd:YAG Laser (Coherent CompassTM215 M-50), which was focused by a 3.5 cm focal length lens. The laser beam waist at the focus is measured to be 15.84 μm and the Rayleigh length is 1.48 mm. A 1 mm wide optical cell containing the 2A6MPS sample in DMF is translated across the focal region along the axial direction that is the direction of the propagation laser beam. The transmission of the beam through an aperture placed in the far field was measured using photo detector fed to the digital power

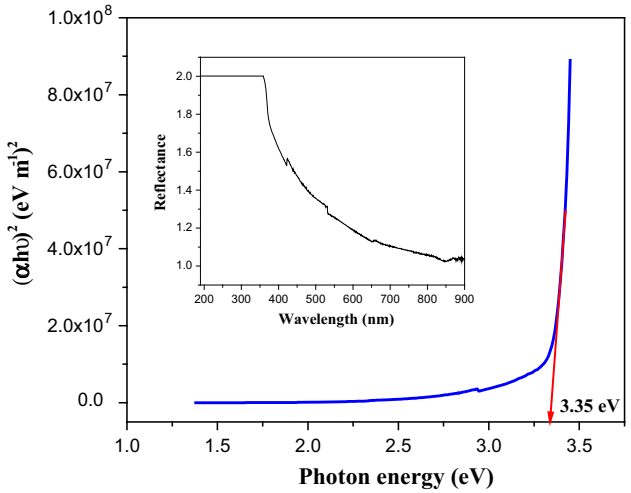

Fig. 11 Plot of (αhν)2 versus photon energy of 2A6MPS crystal. *Inset* shows the reflectance as a fuction of wavelength

meter (Field master GS-coherent). For an open aperture *Z*-scan, a lens to collect the entire laser beam transmitted through the sample replaced the aperture. Figure 12(a), (b) and (c) gives a closed, open and ratio of the closed-to-open normalized *Z*-scan of 2A6MPS sample in DMF at 60 % transmittance.

The peak followed by a valley-normalized transmittance obtained from the closed aperture *Z*-scan data indicates that the sign of the refraction nonlinearity is negative, i.e., self-defocusing. The self-defocusing effect is due to the local variation in the refractive index with the temperature.

The measurable quantity $\Delta T_{p\text{-}v}$ can be defined as the difference between the normalized peak and valley transmittances, $T_p - T_v$. The variation of this quantity as a function of $|\Delta\phi_o|$ is given by

$$\Delta T_{p-v} = 0.406(1-S)^{0.25}|\Delta\phi_o| \quad (5)$$

where $\Delta\phi_0$ is the on-axis phase shift at the focus. S the aperture linear transmittance is given by

$$S = 1 - \exp\left(-2r_a^2/\omega_a^2\right) \quad (6)$$

with r_a denoting the aperture radius and ω_a denoting the radius of the laser spot before the aperture .

The on-axis phase shift is related to the third order nonlinear refractive index (n_2) [24] by,

$$|\Delta\phi_0| = kn_2L_{eff}I_0 \quad (7)$$

where $L_{eff} = (1 - e^{-\alpha L})/\alpha$, with L the sample length, α is the linear absorption coefficient I_O is the intensity of the laser beam at focus $z = 0$, and k is the wave number($k = 2\pi/\lambda$)

The imaginary parts of the third-order nonlinear optical susceptibility [χ^3] is estimated using the value of the nonlinear absorption coefficient β obtained from the open aperture Z-scan data and using the relations:

$$q_o(z) = \frac{\beta \cdot I_o \cdot L_{eff}}{\left(1 + \frac{Z^2}{Z_o^2}\right)} \quad (8)$$

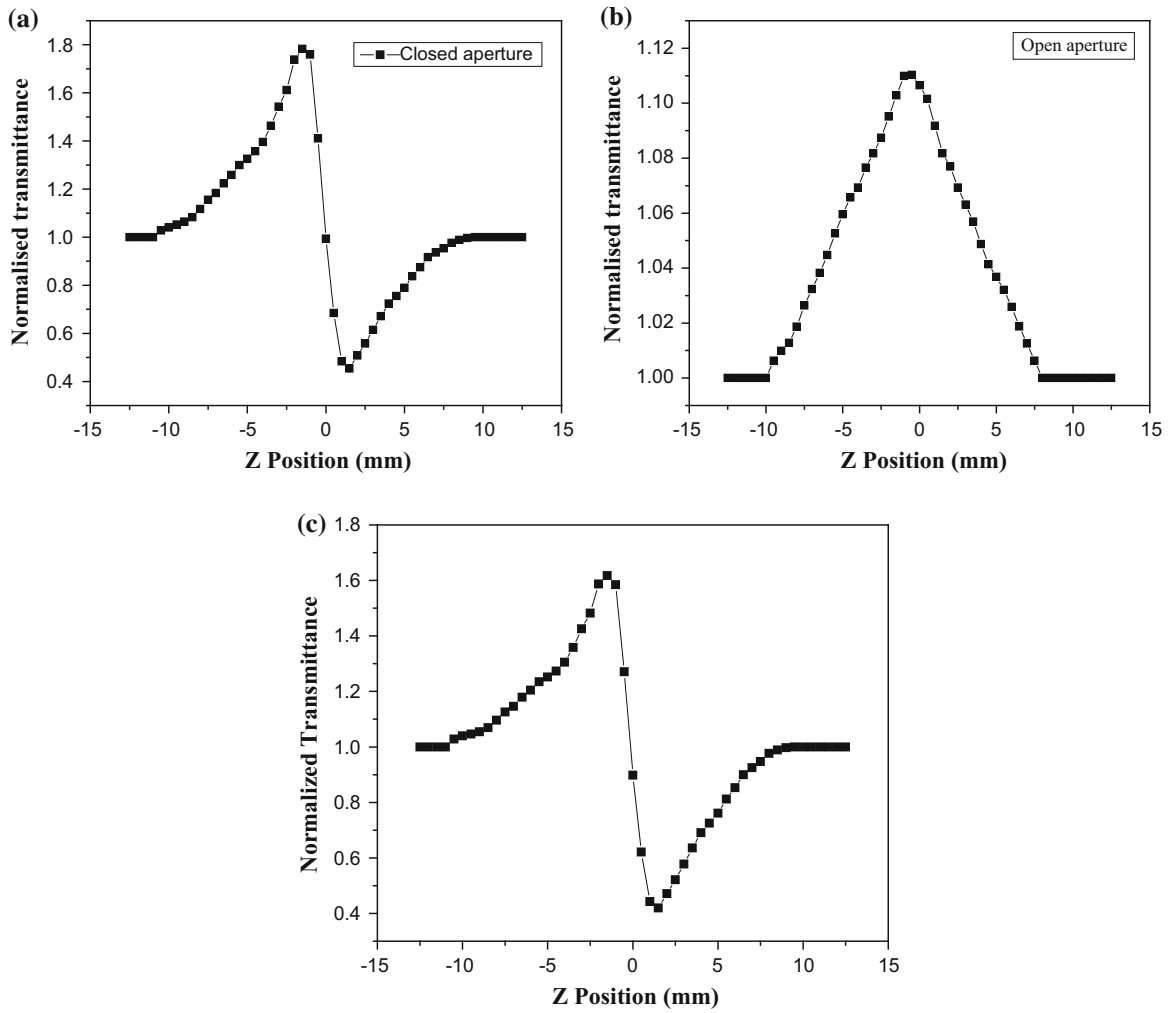

Fig. 12 **a** Closed aperture, **b** Open aperture and **c** Ratio of the closed-to-open Z-scan curves

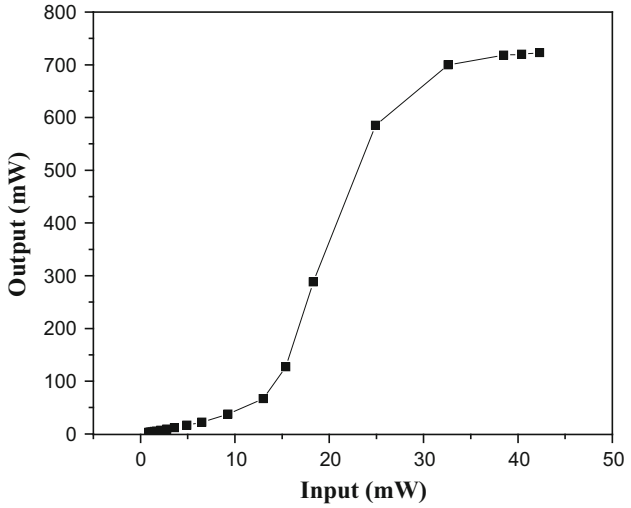

Fig. 13 Optical limiting curve of 2A6MPS crystal

$$\beta = \frac{2\sqrt{2} \cdot \Delta T}{I_o \cdot L_{eff}} \tag{9}$$

$Z_R = k\omega_0^2/2$ is the diffraction length of the beam, ω_0 is the beam waist radius at the focal point.

Experimentally determined nonlinear refractive index n_2 and nonlinear absorption coefficient β can be used in finding the real and imaginary parts of the third-order nonlinear optical susceptibility [χ^3] [25] according to the following relations.

$$\mathrm{Re}\chi^3(esu) = 10^{-4}\frac{\varepsilon_o c^2 n_o^2}{\pi} n_2\left(\frac{cm^2}{W}\right) \tag{10}$$

$$I_m\chi^3(esu) = 10^{-2}\frac{\varepsilon_o c^2 n_o^2 \lambda}{4\pi^2}\beta\left(\frac{cm}{W}\right) \tag{11}$$

where ε_0 is the vacuum permittivity, and c is the light velocity in vacuum.

The absolute value of the third-order nonlinear optical susceptibility is given by the relation

$$|\chi^3| = \left[(R_e(\chi^3))^2 + (I_m(\chi^3))^2\right]^{1/2} \tag{12}$$

The calculated nonlinear refractive index (n_2), absorsption coefficient (β) and third order susceptibility ($\chi^{(3)}$) values are 3.1446×10^{-6} cm^2/W, 7.352×10^{-3} cm/W and 1.5642×10^{-4} esu, respectively. The nonlinear absorption can be attributed to a saturation absorption process and the nonlinear refraction leads to the self-defocusing in this crystal. Figure 13 shows the optical limiting curve for 2A6MPS crystal. The output intensity increases almost linearly with increase in input intensity up to 24.9 mW. The output intensity deviates from the linearity above 24.9 mW and starts to attain saturation. The results are quite interesting for possible nonlinear optical devices such as the prevention of optical damage to very sensitive sensors and eyes [26].

Conclusions

A novel organic 2A6MPS compound was synthesized successfully and crystals grown by the slow evaporation technique. Single crystal X-ray diffraction study revealed the crystal structure of 2A6MPS compound. UV–Vis–NIR spectral study showed the optical quality of 2A6MPS crystal with a lower cut-off wavelength 356 nm. TG/DT analyses revelaed that the grown crystal is stable up to 161 °C. From the Z-scan study, nonlinear refractive index (n_2), absorption coefficient (β) and third order susceptibility ($\chi^{(3)}$) values were calculated to be 3.1446×10^{-6} cm^2/W, 7.352×10^{-3} cm/W and 1.5642×10^{-4} esu, respectively.

References

1. G.R. Desiraju, Engineering: from molecule to crystal. J. Am. Chem. Soc. **135**, 9952 (2013)
2. B. Ruiz, M. Jazbinsek, P. Günter, Handbook of organic materials for optical and (opto) electronic devices. Cryst. Growth Des. **8**, 4173 (2008)
3. L.L. Wen, Z.D. Lu, X.M. Ren, C.Y. Duan, Q.J. Meng, S. Gao, A two-dimensional rare earth metal-organic polymer with 3-carboxylate-4-sulfonatophenolate ligands. Cryst. Growth Des. **9**, 227 (2009)
4. M. Dhavamurthy, G. Peramaiyan, R. Mohan, Synthesis, growth, structural, thermal, dielectric and mechanical studies of an organic guanidinium p-nitroohenolate crystal. J. Cryst. Growth **399**, 13 (2014)
5. P.V. Dhanaraj, N.P. Rajesh, J. Kalyana Sundar, S. Natarajan, G. Vinitha, Studies on growth, crystal structure and characterization of novel organic nicotinium trifluoroacetate single crystals. Mater. Chem. Phys. **129**, 457 (2011)
6. S. Manivannan, S. Dhanuskodi, K. Kirschbaum, S.K. Tiwari, Design of an efficient solution grown semiorganic NLO crystal for short wavelength generation: 2-amino-5-nitropyridinium tetrafluoroborate. Cryst. Growth Des. **5**, 1463 (2005)
7. Bruker APEX2, SAINT, XPREP and SADABS, Bruker AXS Inc., Madison, Wisconsin, USA (2004)
8. G.M. Sheldrick, A short history of SHELX. Acta Cryst. **64**, 112–122 (2008)
9. F.P. Anderson, J.F. Gallagher, P.T.M. Kenny, A.J. Lough, Bis(4-amino-pyridinium) tetra-chlorido-cobaltate(II). Acta Cryst. **61**, o1351–o1353(2005)
10. K.S.S. Babu, G. Peramaiyan, M. NizamMohideen, R. Mohan, Crystal structure of 2-amino-5-nitro-pyridinium sulfamate. Acta Cryst. **70**, o391–o392 (2014)
11. K. Syed Suresh Babu, G. Peramaiyan, M. NizamMohideenb, R. Mohana, 2-Amino-6-methyl-pyridinium 4-methyl-benzene-sulfonate. Acta Cryst. **70**, o600–o601 (2014)
12. M.A. Rajkumar, S.S.J. Xavier, S. Anbarasu, P.A. Devarajan, M. NizamMohideen, 2-Amino-5-nitro-pyridinium hydrogen oxalate. Acta Cryst. **70**, 473 (2014)

13. J. Bernstein, R.E. Davis, L. Shimoni, N.L. Chang, Patterns in hydrogen bonding: functionality and graph set analysis in crystals. Angew. Chem. Int. Ed. Engl. **34**, 1555 (1995)
14. O. Allen, F.H. Kennard, D.G. Watson, L. Brammer, A.G. Orpen, R. Taylor, Table of bond lengths determined by X-ray and neutron diffraction. J. Chem. Soc. Perkin Trans. **2**, 1 (1987)
15. I. Nahringbauer, A. Kvick, 2-Amino-5-methylpyridine. Acta Cryst. **33**, 2902 (1977)
16. H. Ishikawa, K. Iwata, H. Hamaguchi, Picosecond dynamics of stepwise double proton-transfer reaction in the excited state of the 2-aminopyridine/acetic acid system. J. Phys. Chem. **106**, 2305 (2002)
17. Z.M. Jin, Y.J. Pan, M.L. Hu, L. Shen, Crystal structure of 2-amino-3-methylpyridinium ortho-phthalate. J. Chem. Crystallogr. **31**, 191 (2001)
18. C. Balarew, R. Dehlew, Application of the hard and soft acids and bases concept to explain ligand coordination in double salt structures. J. Solid State Chem. **55**, 1 (1984)
19. G. Peramaiyan, P. Pandi, R. Mohan Kumar, Bulk growth, optical, thermal, dielectric and mechanical studies of nonlinear optical crystal Triethylaminium picrate. J. Therm. Anal. Calorim. **9**, 119 (2015)
20. B.M. Sornamurthy, G. Peramaiyan, P. Pandi, S. Das, G. Bhagavannarayana, V. Manivannan, R. MohanKumar, Studies on the growth, thermal and optical properties of 4-aminopyridinium p-aminobenzoate dihydrate single crystals. J. Cryst. Growth **397**, 1 (2014)
21. G.C. Bhar, R.C. Smith, Phys. Status Solidi **13**, 157 (1972)
22. G. Peramaiyan, G. Bhagavannarayana, R. Mohan Kumar, Crystal growth, structural, optical and dielectric studies of ammonium p-toluenesulfonate. J. Cryst. Growth **408**, 14 (2014)
23. M. Sheik-Bahae, A.A. Said, T.H. Wei, D.J. Hagan, E.W. Van stryland, Sensitive measurement of optical nonlinearities using a single beam. IEEE J. Quantum Electron. **26**, 760 (1990)
24. T.D. Krauss, F.W. Wise, Femtosecond measurement of nnonlinear absorption and refraction in CdS, ZnSe and ZnS. Appl. Phys. Lett. **65**, 1739 (1994)
25. T. Cassano, R. Tommasi, M. Ferrara, F. Babudri, G.M. Farinola, F. Naso, Substituent-dependence of the optical nonlinearities in poly(2,5-dialkoxy-*p*-phenylenevinylene) polymers investigated by the *Z*-scan technique. Chem. Phys. **272**, 111 (2001)
26. N. Ramamurthy, S. Dhanuskodi, M.V. Manjusha, J. Philip, Low power CW optical limiting properties of bis(2-aminopyridinium)-succinate-succinic acid (2APS) single crystal. Opt. Mater. **33**, 607 (2011)